Geochimica et Cosmochimica Acta 355 (2023) 75–88

Contents lists available at ScienceDirect

Geochimica et Cosmochimica Acta

journal homepage: www.elsevier.com/locate/gca

Fossil micrometeorites from Monte dei Corvi: Searching for dust from the Veritas asteroid family and the utility of micrometeorites as a palaeoclimate proxy

M.D. Suttle [a,b,c,*], F. Campanale [d], L. Folco [b,e], L. Tavazzani [f], M.M.M. Meier [g], C.G. Miller [h], G. Hughes [c], M.J. Genge [i], T. Salge [j], J. Spratt [j], M. Anand [a]

[a] School of Physical Sciences, The Open University, Walton Hall, Milton Keynes MK7 6AA, UK
[b] Dipartimento di Scienze della Terra, Università di Pisa, 56126 Pisa, Italy
[c] Planetary Materials Group, Natural History Museum, Cromwell Road, London SW7 5BD, UK
[d] Dipartimento di Scienze dell'Ambiente e Della Terra, Università degli Studi di Milano-Bicocca, Piazza dell'Ateneo Nuovo, 1 - 20126 Milano, Italy
[e] CISUP, Centro per l'Integrazione della Strumentazione dell'Università di Pisa, Lungarno Pacinotti 43, 56126 Pisa, Italy
[f] Institute of Geochemistry and Petrology, ETH Zurich, Clausiusstrasse 25, 8092 Zurich, Switzerland
[g] Naturmuseum St.Gallen, Rorschacher Strasse 263, CH-9016 St. Gallen, Switzerland
[h] Department of Palaeontology, The Natural History Museum, London, UK
[i] Department of Earth Science and Engineering, Imperial College London, South Kensington, London SW7 2AZ, UK
[j] Imaging and Analysis Centre, Natural History Museum, Cromwell Road, London SW7 5BD, UK

ARTICLE INFO

Associate editor: Yves Marrocchi

Keywords:
Micrometeorites
Asteroids
Veritas
Fossilisation
Palaeoclimate

ABSTRACT

We searched late Miocene sedimentary rocks in an attempt to recover fossil micrometeorites derived from the Veritas asteroid family. This study was motivated by the previous identification of a pronounced ^{3}He peak (4-5x above background) within marine sediments with ages between ~8.5–6.9 Ma ago (Montanari et al., 2017. GSA Bulletin, 129:1357–1376). We processed 118.9 kg of sediment from the Monte dei Corvi beach section (Italy), the global type-section for the Tortonian epoch (11.6–7.2 Ma). Samples were collected both before and within the ^{3}He peak. Although a small number of iron-rich (I-type) fossil micrometeorites were recovered from each horizon studied (N_{total} = 20), there is no clear difference between the pre- and intra- ^{3}He peak samples. All micrometeorites are compositionally similar, and three out of five horizons yielded similar abundances and particle sizes. Micrometeorites extracted from sediments at the base of the ^{3}He peak were exclusively small (ø <75 μm), while micrometeorites extracted from sediments near the highest ^{3}He values were relatively large (ø <270 μm). The recovered fossil micrometeorites are interpreted as samples of the background dust flux derived from metal-bearing chondritic asteroids. The presence of a ^{3}He signature combined with the absence of fossil micrometeorites or extraterrestrial spinels (Boschi et al., 2019, Spec. Pap. Geol. Soc. Am. 542:383–391) unambiguously related to the Veritas event suggests that the Veritas family is composed of highly friable materials that rarely survive on the sea floor to become preserved in the geological record. Our data supports the existing hypothesis that the Veritas asteroid family is an aqueously altered carbonaceous chondrite parent body, one that contains minimal native metal grains or refractory Cr-spinels. The low yield of fossil micrometeorites at Monte dei Corvi is attributed to loss of particles by dissolution whilst they resided on the sea floor but also due to high sedimentation rates leading to dilution of the extraterrestrial dust flux at this site. As with other fossil micrometeorite collections (e.g. Cretaceous chalk [Suttle and Genge, EPSL, 476:132–142]) the I-type spherules have been altered since deposition. In most particles, both magnetite and wüstite remain intact but have been affected by solid state geochemical exchange, characterised by partial leaching of Ni, Co and Cr and implantation of Mn, Mg, Si and Al. In some particles Mn concentrations reach up to 16.6 wt%. Conversely, in some micrometeorites wüstite has been partially dissolved, or even replaced by calcite or ankerite. Finally, we observe evidence for wüstite recrystallisation, forming a second generation of magnetite. This process is suggested to occur by oxidation during

* Corresponding author at: School of Physical Sciences, The Open University, Walton Hall, Milton Keynes MK7 6AA, UK.
E-mail addresses: martin.suttle@open.ac.uk (M.D. Suttle), fabrizio.campanale@unimib.it (F. Campanale), luigi.folco@unipi.it (L. Folco), lorenzo.tavazzani@erdw.ethz.ch (L. Tavazzani), matthias.meier@naturmuseumsg.ch (M.M.M. Meier), g.miller@nhm.ac.uk (C.G. Miller), g.hughes@nhm.ac.uk (G. Hughes), m.genge@ic.ac.uk (M.J. Genge), t.salge@nhm.ac.uk (T. Salge), j.spratt@nhm.ac.uk (J. Spratt), mahesh.anand@open.ac.uk (M. Anand).

https://doi.org/10.1016/j.gca.2023.06.027
Received 22 December 2022; Accepted 26 June 2023
Available online 29 June 2023

residence on the seafloor and has implications for the use of fossil I-type micrometeorites as a potential proxy for probing Earth's upper atmospheric composition (oxidative capacity) in the geological past. However, solutions to the limitations of post-depositional recrystallisation are suggested. Fossil I-type spherules remain a potential tool for palaeo-climatic studies.

1. Introduction

The asteroid belt marks the boundary between the inner and outer solar system. It is composed of shattered planetesimals, protoplanets and primitive nebula accretion products (DeMeo and Carry, 2014; Greenwood et al., 2020). Over the lifetime of the solar system, the asteroid belt has evolved through dynamical interactions with Jupiter, and by impact events (e.g. Morbidelli et al., 2015; Bottke et al., 2015). High-energy collisions between large asteroids led to their catastrophic disruption, producing an abundance of smaller fragments with similar orbital elements – termed asteroid families (Hirayama, 1918; Nesvorný et al., 2002). Major break-up events would have generated huge volumes of cosmic dust, which then spiralled into the inner solar system and were removed on geologically short timescales by collisions with the Sun or terrestrial planets (Nesvorný et al., 2003; 2006; Vokrouhlický et al., 2008). Epochs of enhanced cosmic dust flux arriving on Earth could potentially have affected the atmosphere, climate and biosphere through variations in nutrient supply, aerosol abundance and atmospheric opacity (Lindskog et al., 2017; Reiners and Turchyn, 2018; Schmitz et al., 2019a; Rudraswami et al., 2021).

Analysis of the asteroid belt's dynamical structure and size-frequency distribution provides insights into its collisional history, including estimates for the timing of major break-up events (e.g. Bottke et al., 2015; Spoto et al., 2015; Delbo et al., 2019). The most significant event in the last 500 Ma appears to have been the formation of the L chondrite Gefion asteroid family (~467 Ma). This event delivered huge volumes of material to Earth, some of which was preserved in Ordovician sediments as fossil meteorite and micrometeorites (Schmitz et al., 1996; 1997; 2014; Meier et al., 2010) and detrital extraterrestrial Cr-spinel (~$FeCr_2O_4$) grains, weathered out of extraterrestrial hosts (Schmitz and Häggström, 2006; Greenwood et al., 2007). Today, approximately two thirds of L chondrite meteorites found on Earth have shock ages consistent with the Gefion family formation event, attesting to the long-term significance of large-scale asteroid impacts (Korochantseva et al., 2007; Nesvorný et al., 2009).

The Veritas asteroid family is a collisional group that formed 8.7–8.3 Ma ago (Nesvorný et al., 2003; Tsiganis et al., 2007). It is located in the outer asteroid belt (~3.16 AU) and contains 1394 members, of which ~300 have diameters >1 km (Nesvorný et al., 2003). The asteroids of the Veritas family are part of the *Ch* near-IR spectral class and are, therefore, associated with carbonaceous chondrites (DeMeo et al., 2009; Ziffer et al., 2011). There is evidence for hydration among some of the Veritas members (detection of the 0.7 μm feature in visible-IR reflectance spectra, corresponding to potential M—OH bonds in phyllosilicates), implying these asteroids may be related to the hydrated CM, CR or CI carbonaceous chondrite groups (Fornasier et al., 2014; Kaluna et al., 2016). Prior to disruption the Veritasian parent body is estimated to have been between 112 and 140 km in diameter (Nesvorný et al., 2003; Michel et al., 2011).

The young age of the Veritas family, and the presence of a Zodiacal dust band associated with this family implies that Veritas material could be present among the micrometeorite flux reaching Earth today (Nesvorný et al., 2003). Furthermore, the flux of Veritas dust is expected to have been significantly higher ~8 Ma ago (Vokrouhlický et al., 2008). Several studies have, therefore, searched late Miocene rocks for evidence of an enhanced cosmic dust flux. Farley et al. (2006) measured ^{3}He abundances (an isotopic proxy for extraterrestrial dust flux [Merrihue, 1965; Farley, 1995; Stuart and Lee, 2012]) in deep sea sediments spanning the last 70 Ma. They identified a peak (4x above background level) in Miocene rocks (~8.2 Ma) and suggested this was due to the Veritas break-up event. Subsequent studies have independently confirmed the presence of the Miocene ^{3}He spike (Montanari et al., 2017). Montanari et al. (2017) conducted a high-resolution survey over this time period and reported a fivefold ^{3}He anomaly starting at 8.47 ± 0.05 Ma and returning to background values at ~6.9 Ma. They identified four pulses during the ^{3}He anomaly, implying that the delivery of Veritas dust to Earth occurred as a series of successive high-flux, short duration events. In addition, Montanari et al. (2017) observed a correlation between ^{3}He abundance and the bulk $\delta^{18}O$ composition of the host sediments, suggesting a link between enhanced dust delivery and the well-documented period of Miocene global cooling (Herbert et al., 2016).

Later, Boschi et al. (2019) performed acid dissolution on 100 kg of marine sediments from within the elevated ^{3}He anomaly, searching for detrital extraterrestrial Cr-spinel grains. These occur as accessory minerals in many different meteorite groups. They have diagnostic trace element chemistries and O-isotope compositions (Schmitz et al., 2019b; Greenwood et al., 2007; Heck et al., 2010), and due to their highly resistant mineralogy often survive atmospheric entry, burial and diagenesis. This is in contrast to the bulk mineralogy of chondritic meteorites, which rarely survive in the terrestrial rock record (Schmitz and Häggström, 2006; Schmitz et al., 2019b). Boschi et al. (2019) found 1151 Cr-spinel grains but concluded that none had extraterrestrial origins. They suggest this supports the link between the ^{3}He anomaly and a carbonaceous chondrite parent body, because the abundance of Cr-spinel is low in carbonaceous chondrites, relative to the high abundances found in ordinary chondrites and achondritic meteorites.

To date no fossil micrometeorites have been recovered from Miocene sediments. Previous studies investigating the Monte dei Corvi beach section used harsh processing methods, relying on strong acids (e.g. hydrofluoric acid) to dissolve the host sediments (e.g. Boschi et al., 2019). However, these will have also dissolved any fossil micrometeorites present within these rocks composed of silicates, sulphides, metal or magnetite. By contrast, studies focused on other time periods and using more moderate extraction techniques (weaker acids or mechanical disaggregation) have successfully recovered fossil micrometeorites from a range of sediment types (e.g. Mutch 1965; Taylor and Brownlee, 1991; Onoue et al., 2011; Tomkins et al., 2016; Suttle and Genge, 2017; Kadyrov et al., 2020). In this study we aimed to recover and characterise fossil micrometeorites from the Veritas asteroid family by processing late Miocene sediments from the Tortonian type section at Monte dei Corvi in Italy.

2. Geological Setting: Monte dei Corvi

The Monte dei Corvi beach section (43°35′14.5″N, 13°33′58.1″E) is located ~6 km southeast of Ancona, Italy. It is the global stratotype section and point (GSSP) for the base of the Tortonian (11.6 Ma) (Hilgen et al., 2005; Hüsing et al., 2009a). Here, along the coastline, an extensive outcrop (>200 m) of pelagic carbonate rock is exposed. They span the late Serravallian, the entire Tortonian and parts of the Messinian – a time range of approximately 13.0 to ~6.8 Ma ago (Montanari et al., 1997; Hilgen et al., 2003; 2005; Hüsing et al., 2009a; Wotzlaw et al., 2014). The cliff front is composed of grey and white marls, interbedded with darker brown-black organic-rich sapropel deposits, forming rhythmic cycles within a deep-sea basin environment. They are interpreted as orbitally forced (Milankovitch cycle) climatic fluctuations, with precession, obliquity and eccentricity all evident in the sedimentary succession (Cleaveland et al., 2002; Hüsing et al., 2009a). In total, 203

cycles are recognized (Hilgen et al., 2005). The Serravallian/Tortonian boundary (GSSP, 11.63 Ma) occurs at the mid-point of cycle 76 and is defined by the disappearance of calcareous nannofossils *Discoaster kugleri* and *Globigerinoides subquadratus* (Hilgen et al., 2005).

The regional geological sequence across much of the Umbria-Marche basin was affected by tectonic faulting and the injection of siliclastic turbidite sequences of the Marnoso-Arenacea Flysch (Montanari et al., 1997; 2017; Hilgen et al., 2003; 2005). However, the Monte dei Corvi exposure avoided these overprints and is, therefore, the most complete late Miocene succession in the Mediterranean (Hilgen et al., 2005; Hüsing et al., 2009a). At Monte dei Corvi, larger, non-repetitive stratigraphic changes are overlain upon the smaller-scale cyclic variations and allow the outcrop to be subdivided. These intervals are termed: Marl-Sapropels, Marly, Brownish, Rossini and Euxinic Shale horizons (Hüsing et al., 2009a). They represent regional environmental changes driven primarily by tectonic events. The main ^{3}He anomaly occurs within the Marly and Brownish units (8.5–6.9 Ma, Montanari et al., 2017). Sedimentation rates over the time frame investigated in this study vary from ~1.9 cm/ka at 8.7 Ma to 1.1 cm/ka at 7.9 Ma (Hüsing et al., 2009a).

3. Methods

3.1. Samples

We sampled five horizons (here termed A-E) within the Monte dei Corvi beach section. Two samples (A and B) were located below the base of the ^{3}He peak, while the remaining three samples (C-E) are within the ^{3}He peak (Fig. 1. and Table 1). At each horizon >20 kg of rock was extracted from a stratigraphic thickness of <20 cm. Rock samples were transported to the Dipartimento di Scienze della Terra at the Università di Pisa where they were processed for micrometeorite extraction.

3.2. Micrometeorite search and extraction

We opted to use a combination of crushing and magnetic separation instead of acid dissolution for four reasons: (1) previous tests on Cretaceous chalk (Suttle and Genge, 2017) found that crushing and magnetic separation yielded significantly more micrometeorites than acid dissolution. This was because clay fines within the acid-insoluble residue formed a compact slurry that effectively prevented micrometeorite extraction. (2) The majority of micrometeorites are magnetic (Suavet et al., 2009a), owing to the presence of Fe-Ni-metal and/or magnetite meaning that liberation from the host rock and magnetic separation should be an effective recovery approach. (We note that the inability to recover non-magnetic glassy (V-type) cosmic spherules is a drawback of our approach). (3) Acid dissolution on the scale required in this study (>100 kg) carries significant health and environmental hazards. (4) Acid dissolution techniques were previously applied to these sediments in the study of Boschi et al. (2019).

All rock samples were dry processed using a jaw crusher (Fig. S1B) to produce powders with grain sizes < 2 mm diameter. A nominal grain size of 2 mm is close to, but larger than, the expected size of any potential micrometeorite (e.g. Suavet et al., 2009b) and, therefore, struck a balance between avoiding micrometeorite damage during rock processing and promoting micrometeorite liberation from the host sediment. The resulting rock powders were then passed (twice) through a high-efficiency magnetic separator (S+S Extractor-SE produced by Separation and Sorting Technology GmbH) (Fig. S1C). All equipment was thoroughly cleaned between samples to avoid contamination. The magnetic fraction of each sample was subsequently searched under optical microscope and potential micrometeorites removed and imaged under scanning electron microscope (SEM) before being embedded in epoxy resin (EpoFix) and sectioned to expose their interiors. The sectioned particles were carbon coated and re-imaged under SEM allowing analysis of their internal textures, mineralogy, and chemical compositions.

In addition, we performed a survey of the non-magnetic fraction to determine whether additional micrometeorites or other objects of interest were present in the Monte dei Corvi sediments. Previous studies have demonstrated that glassy V-type spherules are the only fraction of the cosmic spherule population that are not magnetic (Taylor et al., 2000; Suavet et al., 2009a). We searched approximately 30 g of the non-magnetic material in each of the five horizons (A-E). To remove the finest size fractions (approximately < 10 μm) that adhere to the margins of larger grains and make optical searching difficult we washed these subsample aliquots in water. This was achieved by stirring the water–sediment mixture and leaving the container for ~10 s – allowing the high-density particles to settle to the base of the container while the lower density particles remained in suspension and were then poured away. This process was repeated five times before the remaining sediment was dried in an oven at 50 °C for 24 h. The nonmagnetic subsamples were then searched under binocular microscope (Fig. S2). Finally, we also studied the smallest size fractions (<63 μm) to determine if any interplanetary dust particles (IDPs), whose particle diameters are defined as D < 50 μm (Mackinnon and Rietmeijer, 1987)

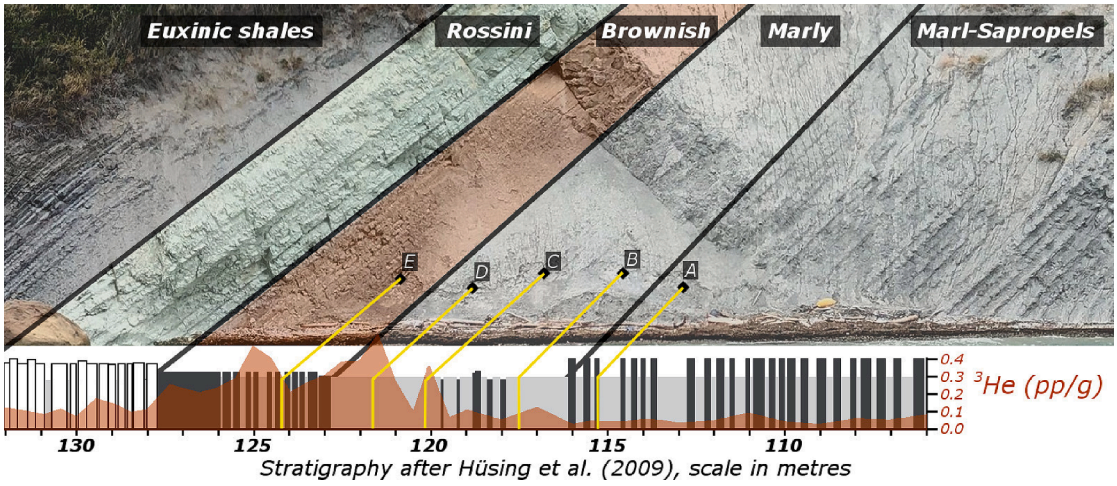

Fig. 1. Panoramic view of the Monte dei Corvi beach section (imaged 30/09/2022) and overlain by interpretation of stratigraphy and geological boundaries (after Hüsing et al. (2009a)). The location of the five sedimentary horizons investigated in this study (samples A-E) are marked by black diamonds and labelled. Yellow lines correlate the position of the samples against the ^{3}He trace reported by Montanari et al. (2017). Samples A and B predate the ^{3}He peak, while samples C, D and E are within the ^{3}He peak with sample D close to the highest ^{3}He abundances.

Table 1
Overview of the five sedimentary horizons studied in this work (samples A-E). The number and inferred mass of micrometeorites recovered from each horizon is shown. This is compared against the mass of terrestrial host rock that was processed, allowing calculation of the preserved fossil micrometeorite mass (μg) per kilogram of terrestrial sediment.

Sample	Geologic Subunit	Relative position	Mass collected (kg)	Mass processed [powder <2 mm] (kg)	No. of MMs	Avg. MM diameter ± 1σ (μm)	No. of MMs/kg	(Inferred) total MM mass (μg)	(Inferred) relative MM mass (μg/kg)	sample/ background relative mass flux
A	*Marl-Sapropels*	Before ^{3}He peak	29.1	23.5	4	118 ± 13	0.17	17.8	0.8	Background: 0.7
B	*Marls*		31.3	28.7	2	137 ± 59	0.07	17.0	0.6	
C	*Marls*	Within ^{3}He	23.3	19.9	7	45 ± 14	0.35	2.2	0.1	0.2
D	*Marls*	peak	29.2	26.2	5	169 ± 80	0.19	97.2	3.7	5.3
E	*Brownish*		24.1	20.6	2	153 ± 23	0.10	19.4	0.9	1.3
		Total	*137.0*	*118.9*	*20*	*Avg: 124*	*Avg: 0.18*	*Avg: 30.7*	*Avg: 1.2*	–

were present in the Monte dei Corvi sediments. This was achieved by spreading a small quantity of the <63 μm powder from two sedimentary horizons (samples A and D) on to carbon tape. These disks were then carbon coated and studied under SEM (Fig. S3).

3.3. Geochemistry

Energy dispersive X-ray spectrometry (EDS) elemental data were collected at the Centro per l'Integrazione della Strumentazione dell'Università di Pisa (CISUP) on a FEI Quanta 450 field emission gun (FEG) SEM fitted with a Bruker Quantax EDS system and XFlash silicon drift detector. This instrument was used to provide a first-pass qualitative assessment of micrometeorite composition and mineralogy and also used to obtain quantitative analyses of small phases (approx. < 5 μm) within the micrometeorites, such as the platinum group nuggets (PGNs) which we were otherwise unable to analyse by wavelengths-dispersive electron microprobe analysers (EMP). We also analysed the host sedimentary rocks using SEM-EDS to obtain approximate bulk chemical compositions (Table S1). This was achieved by repeated, randomly spaced wide-beam analyses on unprocessed rock chips that had been embedded in epoxy resin, sectioned and carbon coated. Standard-less quantitative EDS analysis was obtained under high-vacuum at a fixed working distance of 10 mm with accelerating voltages of 15 kV. Weight totals were determined using the Bruker's built-in interactive PB/ZAF routine with oxygen directly measured. Data are quoted as weight normalized values to one decimal place.

In addition we collected data on a Cameca SX100 EMP based at the Natural History Museum (NHM), London. This was used to quantify the major and minor element compositions of mineral phases (primarily metal, wüstite [$Fe_{(1-x)}O$, where $x < 0.2$] and magnetite [Fe_3O_4]) within the fossil micrometeorites. Analyses were performed using a 20 kV accelerating voltage, a 20 nA beam current and a spot size < 5 μm. Prior to analysis, the instrument was calibrated using suite of mineral standards specific to each element under detection. Cameca PAP matrix correction software was used to remove artefacts arising from atomic number, absorption, and secondary fluorescence (ZAF) effects. Elemental detection limits for this instrument are on the order of 0.02–0.05 wt% and elemental uncertainties vary between 0.01 and 0.03 wt%. For oxides, oxygen was calculated by stoichiometry assuming each cation was in its lowest common valence state (e.g. Fe as Fe^{2+}). Under these assumptions the ideal weight total for magnetite is 93 wt%, while acceptable wüstite analyses exhibit a weight total range between 96 and 100 wt% owing to its variable stoichiometry: $Fe_{(1-x)}O$, where $x < 0.2$ (Darken and Gurry, 1946; Genge et al., 2017).

4. Results

4.1. Host rock bulk chemical composition

Across the stratigraphic sequence investigated (Samples A-E) the host rock bulk chemical composition (Table S1) is dominated by Ca, Si and Al (with high abundances of O [abundance inferred] and C [not measurable by SEM-EDX]). This composition is consistent with a marl, with calcite as the major phase intermixed with a subordinate siliciclastic component. Samples A-D have very similar compositions: Ca (24–32 wt%), Si (16–19 wt%) and Al (6–8 wt%). By contrast Sample E has a slightly different composition with proportionally less calcite (Ca: 17.5 wt%) and a higher siliciclastic component (Si: 21.8 wt% and Al: 8.4 wt%). Across the entire sequence (samples A-E) Fe varies between 2.2 and 3.3 wt% and Ni and Mn are low and uniform at the 0.1 wt% level.

4.2. Micrometeorite textures, mineralogy, and geochemistry

Fossil micrometeorites, found only in the magnetic separates, were recovered from all five horizons (samples A-E) in abundances between 2 and 7 particles per sample (Tables 1 and 2). In total 20 micrometeorites were identified, and, in all instances, these were I-type cosmic spherules composed primarily of Fe-oxides (wüstite and magnetite). Diameters vary between 40 and 270 μm and shapes are close to ideal spheres.

Particle exteriors (Fig. 2 and Fig. S4) show characteristic dendritic textures with a range of morphologies (cruciform, re-entrant, and cellular [Suttle and Genge, 2017]). Additionally, small quantities of Ni- and Cr-rich metal (Table 3, Ni: 18 wt%, Cr: 13 wt%) were observed as

Table 2
Inventory of fossil micrometeorites recovered in this study. Data includes particle IDs, classification into metal-bearing (MET) or fully oxidized (OX) spherules (after Genge et al., 2017), particle diameters (measured from SEM images), the inferred mass of each micrometeorite (calculated assuming all particles are ideal spheres with bulk densities of 5000 kgm^{-3} [Feng et al., 2005]) and the total mass of micrometeorites per sedimentary horizon investigated.

Particle ID	Classification (Genge et al., 2017)	Diameter (μm)	Inferred mass (μg)	Inferred total mass (μg)
A1	OX	107	3.2	17.8
A2	MET	111	3.6	
A3	OX	137	6.7	
A5	OX	118	4.3	
B1	OX	178	14.8	17.0
B2	OX	95	2.2	
C3	MET	75	1.1	2.2
C8	MET	40	0.2	
C9	–	44	0.2	
C10	–	39	0.2	
C11	–	33	0.1	
C12	–	47	0.3	
C13	–	40	0.2	
D1	OX	128	5.5	97.2
D2	OX	157	10.1	
D3	OX	225	29.8	
D4	–	269	51.0	
D5	OX	66	0.8	
E1	OX	169	12.6	19.4
E2	OX	137	6.7	

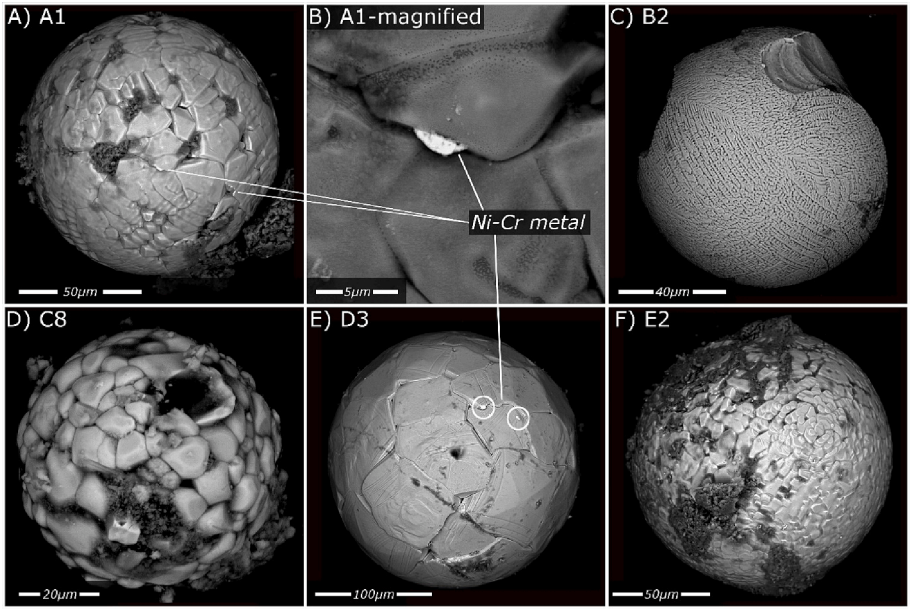

Fig. 2. Example images of fossil micrometeorite exteriors showing their characteristic dendritic textures. Particles were not washed or cleaned by sonication prior to analysis. Fragments of the host sediment (marl) can be seen adhering to the particle surface. In Particle A1 (panel B) small quantities (<10 μm) of Ni-Cr metal are found as growths upon the Fe-oxide dendrites, these are interpreted as deposits of Ni and Cr that were dissolved by terrestrial fluids, and reprecipitated on the particle exteriors.

irregular-shaped growths on the exterior of some micrometeorites (particles A1 [Fig. 2B] and D3 [Fig. 2E]). Note, here, the low abundances of oxygen detected (<6 wt%) in these analyses are likely due to X-ray excitation of the surrounding Fe-oxides phases, or contamination by hydrocarbons.

Particle interiors (Fig. 3 and Fig. S5) are either homogenous (as in particle D3) or contain interlocking dendrites and cavities. As in modern Antarctic I-type spherules the micrometeorites from Monte dei Corvi can be subdivided, based on the classification in Genge et al. (2017) into either metal-bearing (MET), or fully oxidized (OX) spherules. Metal-bearing spherules are identified by the presence of either an intact metal bead (as in particle A2 [Fig. 3A, Fig. 4]), a spherical cavity (as in particle C3 [Fig. 3B] interpreted as the site of a former metal bead that has since been dissolved [van Ginneken et al., 2016; Suttle and Genge, 2017]) or a homogenous wüstite composition (as in particle D5 [Fig. S4]). By contrast, fully oxidised spherules contain significant quantities of magnetite and may also contain wüstite.

Wüstite in the Monte dei Corvi spherules has a variable appearance. In some micrometeorites it occurs as dendrites with well-defined margins (as in particle A2 [Fig. 3A, Fig. 4]), while in other micrometeorites wüstite has an anhedral morphology and porous texture (as in particle B1 [Fig. 3C]). Nickel abundances vary between <0.03 wt% to 4.64 wt%, Cr vary between <0.05 wt% to 0.44 wt%, and Co abundances vary between <0.03 wt% to 0.42 wt% (Table 3). Wüstite compositions generally have low Mn concentrations <0.3 wt%, although in a single micrometeorite (particle A2) Mn concentrations reach 14.2 wt% (Table 3, Fig. 4).

Magnetite is the most abundant mineral phase among the Monte dei Corvi micrometeorite collection and occurs in almost all particles. Magnetite typically has a homogenous appearance (uniform *Z* contrast in back-scattered electron (BSE) images and no voids, cracks, or inclusions). Nickel abundances vary between <0.03 wt% to 4.20 wt%, Cr vary between <0.05 wt% to 0.51 wt% and Co abundances vary between <0.03 wt% to 0.29 wt% (Table 3). Manganese concentrations are low (<0.39 wt%) and generally below detection limits (<0.05 wt%), however, high Mn concentrations (12.23 and 16.60 wt%) were measured in two particles (B2 and C8 respectively, Table 3). These values are similar to the high-Mn wüstite composition found in particle A2.

In three micrometeorites (particles A3, D1 and E2) magnetite was found to coexist not with wüstite but a different phase, either calcite ($CaCO_3$, as in particle A3 [Fig. 3E]), Fe-bearing ankerite ($Ca[Fe][CO_3]_2$, as in particle D1 [Fig. 3F]) or a second generation of magnetite (appearing as smaller, irregular-shaped grains in particle E2 [Fig. 3G]) (Table 3). This occurrence is not found in modern, unweathered Antarctic I-types (Genge et al., 2017) and is, therefore, interpreted as an artefact of terrestrial alteration (and addressed further in the discussion below).

Also present in the Monte dei Corvi micrometeorites are rare submicron PGNs. They were identified in two of the OX spherules (particles A3 and E2) occurring at the interstitial spaces between magnetite and (former) wüstite and appear as bright rounded objects (Fig. 3D). Spot EDX analyses detected Rh, Pt and Au in both particles as well as S in particle A3 (Table 3).

4.3. Changes in the relative micrometeorite mass flux across the sampled horizons

Based on measured particle diameters (40–270 μm) and an assumed bulk density of 5000 kgm^{-3} (Feng et al., 2005) each micrometeorite's inferred mass was calculated (Table 2). Individual masses range from 0.1 to 51.0 μg, while the combined total mass of all micrometeorites recovered is 153.5 μg. Dividing the (inferred) micrometeorite mass by the mass of terrestrial rock searched at each horizon gives a value for the relative abundance of fossil micrometeorites across the stratigraphic section.

The relative micrometeorite abundance in samples A and B (before the ^{3}He peak) is 0.6–0.8 μg/kg, while the relative micrometeorite abundance in samples C, D and E (within the ^{3}He peak) varies between 0.1 and 3.7 μg/kg (Table 1). Sample C (0.1 μg/kg) has the lowest relative micrometeorite mass. Although seven micrometeorites were identified in sample C none have diameters > 75 μm (Table 2). By contrast, in Sample D (3.7 μg/kg), four out of the five micrometeorites found have diameters > 120 μm and this includes the two largest micrometeorites found in this study (D3 and D4, ø >200 μm). Thus, there is a clear size disparity between the micrometeorites recovered in sample C and those found in sample D. Meanwhile sample E (0.9 μg/kg) has an intermediate relative micrometeorite abundance arising from just two relatively large particles (ø: 130–170 μm).

4.4. Other particles in the magnetic separates

In addition to the 20 fossil I-type spherules we identified several

Table 3
Chemical compositions of fossil micrometeorites from Monte dei Corvi (given in unnormalized wt.%). Data is divided into subgroups reflecting the inferred original mineral phase (either metal beads, wüstite, magnetite or [micron-sized] PGNs) that were present when the particle was deposited on the seafloor. Later alteration, either during seafloor residence or during diagenesis resulted in geochemical exchange with surrounding fluids and/or dissolution and replacement by a secondary mineral phase (calcite, ankerite or magnetite). The two most prominent solid-state alteration signatures are the leaching of Ni and implantation of Mn. The "–" symbol is used to denote data that was below detection limit, while the "ND" denotes elements that were not detected in the analysis. (Note: Ni/Co ratios are expressed as wt%/wt% data).

ID	Inferred original phase	Observed composition	Analysis type	N=?	Na	Mg	Al	Si	S	Ca	Ti	Cr	Mn	Fe	Ni	Co	Rh	Pt	Au	O	Total	Ni/Co
A2	Metal bead	Fe-Metal	EMP	5	–	–	–	–	–	–	–	0.06	1.70	95.3	0.32	0.13	ND	ND	ND	ND	97.5	2
D5	Wustite	Wustite (leach. Ni)	EMP	4	–	–	0.07	0.04	0.02	–	–	–	0.28	76.4	–	–	ND	ND	ND	22.1	98.9	N/A
B1	Wustite	Porous wustite	EMP	5	0.07	–	0.07	0.44	0.02	0.11	0.06	–	–	60.9	4.64	0.30	ND	ND	ND	19.5	86.1	15
D2	Wustite	Porous wustite	EMP	4	–	0.04	0.05	0.33	–	0.06	0.05	–	–	56.9	4.43	0.42	ND	ND	ND	18.2	80.4	11
E1	Wustite	Porous wustite	EMP	5	–	–	–	0.23	–	0.19	0.05	0.44	–	57.6	3.27	0.17	ND	ND	ND	18.1	80.0	19
A2	Wustite	Mn-Wustite (leach. Ni)	EMP	6	0.47	0.10	0.90	3.76	0.02	0.47	0.04	0.43	14.2	53.2	–	–	ND	ND	ND	24.8	98.4	N/A
A3	Wustite	Replac. by calcite	EMP	2	–	0.33	–	–	–	37.3	–	–	0.10	4.4	0.12	–	ND	ND	ND	16.7	58.9	N/A
D1	Wustite	Replac. by ankerite	EMP	4	–	0.34	–	–	–	32.0	–	–	0.09	11.2	0.13	0.03	ND	ND	ND	16.5	60.2	4
E2	Wustite	Replac. by magnetite	EMP	2	0.09	–	0.07	0.52	0.04	0.33	0.04	–	–	68.3	0.96	0.32	ND	ND	ND	20.8	91.5	3
A3	Magnetite	Magnetite	EMP	4	–	–	0.14	–	–	0.42	–	–	–	66.7	4.20	0.22	ND	ND	ND	20.6	92.3	19
B1	Magnetite	Magnetite	EMP	5	–	–	–	–	–	–	–	0.20	–	68.0	3.50	0.19	ND	ND	ND	20.6	92.5	18
D2	Magnetite	Magnetite	EMP	4	–	–	0.07	0.05	–	–	0.02	–	–	68.2	3.30	0.27	ND	ND	ND	20.7	92.6	12
E1	Magnetite	Magnetite	EMP	1	–	–	–	–	–	0.13	0.05	0.51	–	68.0	2.78	0.14	ND	ND	ND	20.7	92.2	20
D1	Magnetite	Magnetite	EMP	6	–	0.03	–	0.41	–	4.18	0.03	–	–	64.5	1.05	0.29	ND	ND	ND	21.1	91.6	4
E2	Magnetite	Magnetite	EMP	2	–	–	0.26	–	–	0.06	0.02	0.05	–	71.0	0.60	0.19	ND	ND	ND	20.9	93.0	3
C3	Magnetite	Magnetite	EMP	5	–	–	–	–	–	–	–	–	0.13	70.8	0.04	–	ND	ND	ND	20.4	91.4	N/A
A1	Magnetite	Magnetite	EMP	5	–	–	–	0.13	–	0.02	–	–	0.39	71.1	0.03	–	ND	ND	ND	20.7	92.3	N/A
D3	Magnetite	Magnetite	EMP	4	–	–	–	–	–	–	–	–	0.33	71.9	–	–	ND	ND	ND	20.7	92.9	N/A
B2	Magnetite	Mn-Magnetite	EMP	4	–	–	0.07	0.39	–	–	–	0.37	12.2	58.4	–	–	ND	ND	ND	20.6	92.0	N/A
C8	Magnetite	Mn-Magnetite	EMP	4	–	3.40	0.13	–	–	0.16	–	–	16.6	49.1	–	–	ND	ND	ND	20.8	90.2	N/A
E2	PGN	PGN	EDS	1	–	–	–	–	–	–	–	–	–	42.6	3.3	–	2.4	25.8	4.2	21.7	100.0	N/A
A3	PGN	Sulphidized PGN	EDS	1	–	–	–	–	6.4	–	–	–	–	45.5	4.8	–	3.3	22.2	–	17.9	100.0	N/A
A1	–	Ni-Cr metal	EDS	5	–	–	0.5	1.9	1.0	–	–	12.6	1.0	57.4	18.3	–	–	–	–	6.4	99.0	N/A

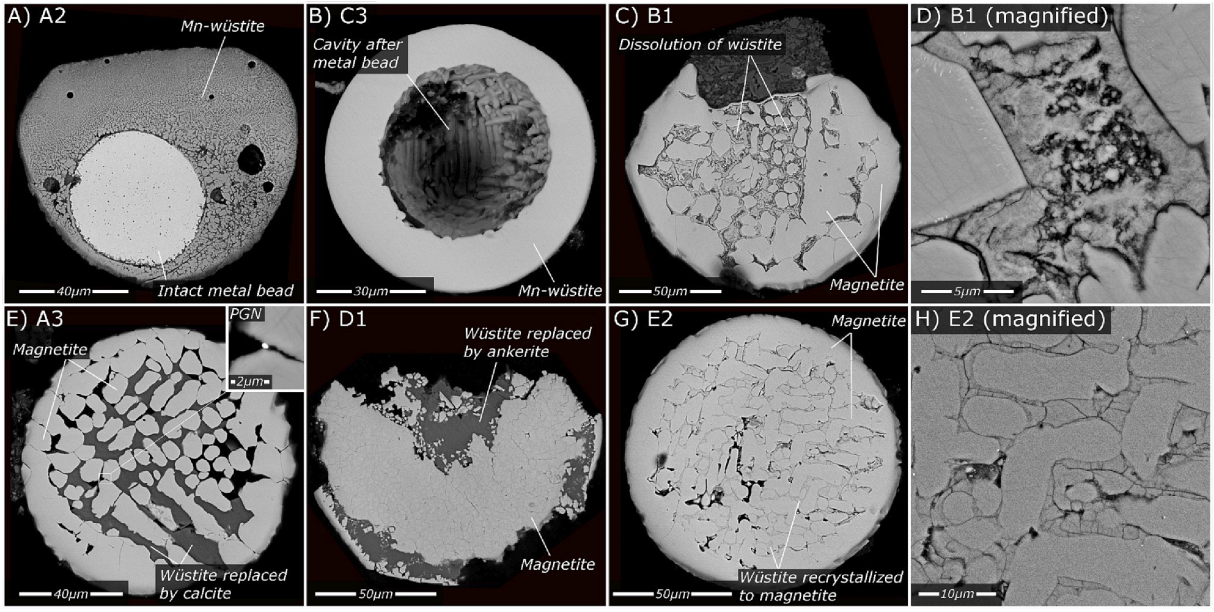

Fig. 3. Example images of fossil micrometeorite interiors highlighting their mineralogy, textures and alteration features. Panels A & B show MET subtypes, particle A2 (panel A) contains an intact metal bead while particle C3 has a spherical cavity reflecting the site of a former metal bead, since dissolved (panel B). Panels C-F show OX subtypes. Particle B1 (panels C and D) shows evidence of partial dissolution of wüstite, while particles A3 and D1 (panels E and F) show instances of complete wüstite dissolution and replacement by carbonate minerals. Particle E2 (panels F and G) demonstrate that wüstite can become recrystallized into a second generation of magnetite, in these instances discerning between pre-depositional and post-depositional magnetite can be difficult, especially if the recrystallization textures were more matured than observed here.

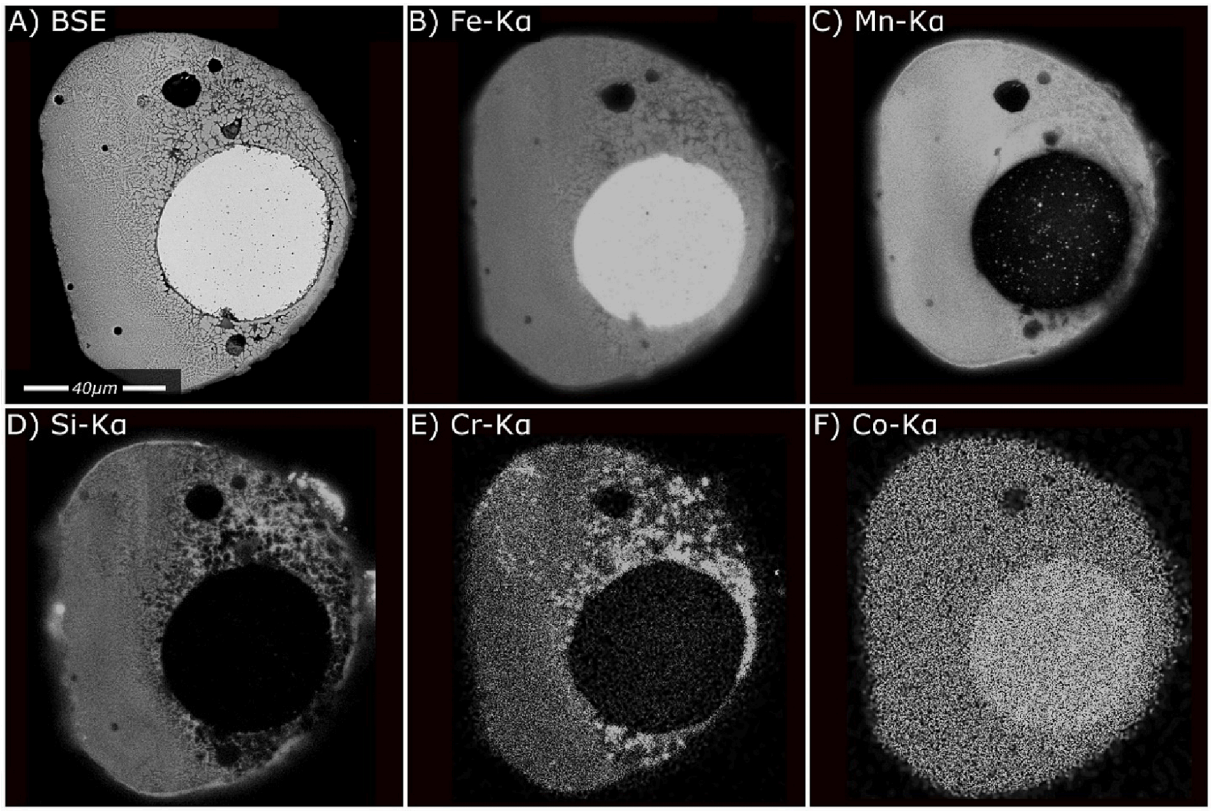

Fig. 4. SEM-EDS maps for particle A2 showing (A) BSE image and (B-F) the spatial distribution of the main elements in particle A2: (B) Fe, (C) Mn, (D) Si, (E) Cr and (F) Co.

other unusual particles. Iron-pyrite (FeS_2) spherules (Fig. 4A and B) and irregular-shaped Fe-sulphide masses (Fig. 5C) were abundant components of the magnetic separate. Under the binocular microscope they appear superficially similar to micrometeorites, however, under the SEM they have framboidal textures, composed of numerous micron-sized crystallites. EMPA revealed an absence of Ni, Co, or Cr (all

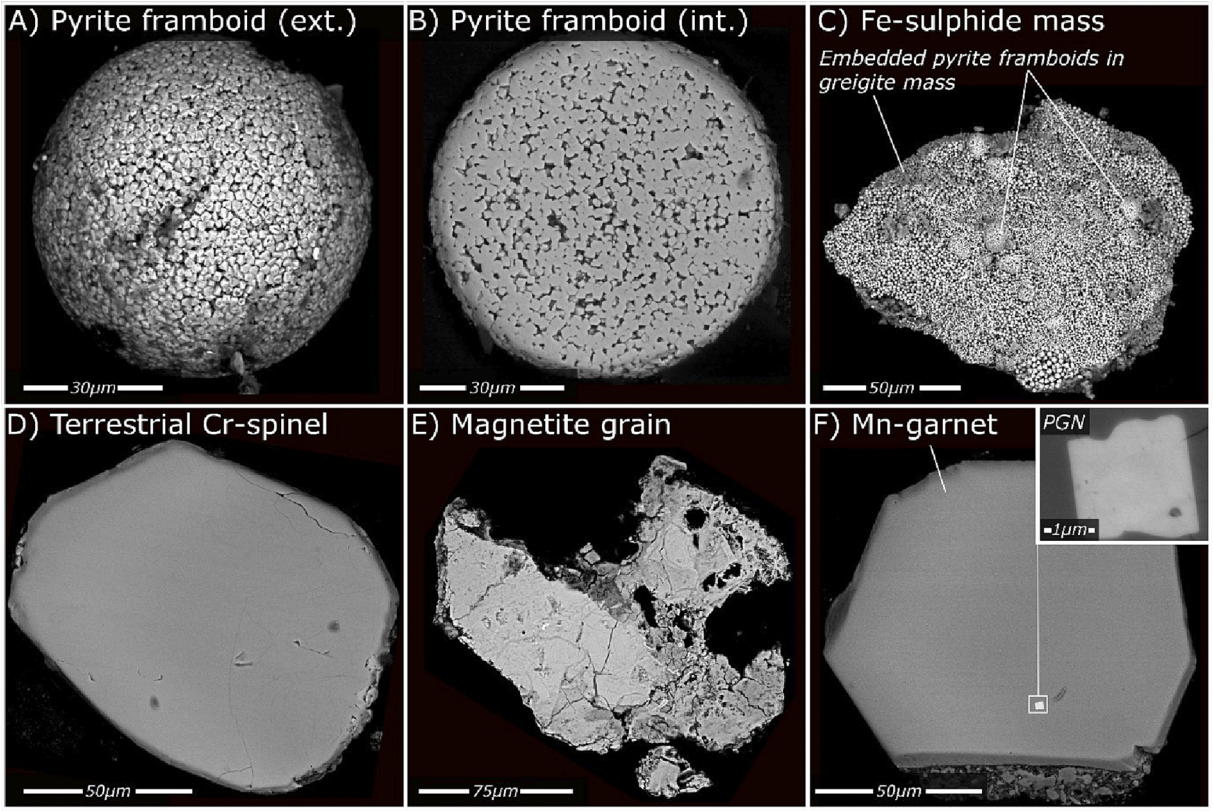

Fig. 5. Examples of other particles found in the magnetic separates. Panels A-C show Fe-sulphide phases, these occur as pyrite spherules with a framboidal textures (panels A and B) or as irregular-shaped masses (panel C) composed of greigite and containing embedded pyrite framboids. The pyrite spherules were common among the Monte dei Corvi magnetic separates. Other phases we identified include a Cr-spinel grain (panel D), a single magnetite grain with a polymineralic texture (panel E) and a Mn-garnet, containing a small, irregular-shaped PGN (panel F). Only the pyrite spherules appear superficially similar to fossil I-type micrometeorites under the binocular microscope.

below detection limits, <0.03–0.05 wt%). Detrital pyrite spherules and greigite (Fe_2S_4) grains were previously identified throughout the Monte dei Corvi stratigraphic section by Hüsing et al. (2009b). They occur both prior to and within the ^{3}He peak and, therefore cannot be related to potential Veritas asteroid dust.

A spinel grain ($X^{2+}Y_2^{3+}O_4$) was identified in sample C (particle C1, 80–115 μm, Fig. 5D). It has a featureless interior and rounded shape. Electron microprobe analysis (N = 4) reveals a cation composition of Cr: 30.5 wt%, Fe: 21.7 wt%, Al: 8.28 wt%, Mg: 5.64 wt%, Ti: 0.47 wt%, Mn: 0.23 wt%, V: 0.19 wt%, and Ni: 0.08 wt%. This composition is inconsistent with extraterrestrial spinels and, instead, matches the composition of terrestrial spinels recovered by Boschi et al. (2019) from the Monte dei Corvi sediments.

We found a single large polymineralic magnetite grain in sample C (particle C7, >150 μm, Fig. 5E). It has an irregular shape and fractured interior. One margin has a fibrous habit indicative of fluid-mediated growth or alteration. Both Co and Cr are below detection limits while Ni occurs as 0.08 wt% and Mn occurs at 0.49 wt%.

A single euhedral garnet grain was identified in sample C (particle C5, >100 μm, Fig. 4F). Its cation composition is dominated by Mn (25.7 wt%) identifying this particle as a Mn-garnet, close to the Mn end-member composition, spessartite ($Mn_3Al_2[SiO_4]_3$.). Interestingly, a small (~2.5 μm) PGN with a rectangular profile and euhedral morphology is also present within the garnet. Spot EDX analyses detected both Pt and Au.

4.5. The non-magnetic fraction

The non-magnetic fraction did not contain extraterrestrial materials. Instead it is dominated of subrounded irregular-shaped grains of carbonate (Fig. S2) and includes numerous well-preserved foraminifera tests, with both planktonic and benthic species present (Fig. S2D). Their preservation undamaged despite liberation from the host rock by crushing demonstrates that the fossil micrometeorite population was also unlikely to have been damaged by the extraction procedure we employed.

Among the smallest size fractions (<63 μm) SEM analysis revealed framboidal Fe-sulphide grain aggregates and euhedral Fe-sulphide crystals (identical to those shown in Fig. 5). In addition we identified rare instances of small barium sulphate grains (Fig. S3) and detrital zircon crystals (<5 μm) contained within carbonate grain aggregates. No extraterrestrial IDP grains were identified.

5. Discussion

5.1. Lack of unmelted and S-type micrometeorites

The lack of unmelted micrometeorites or silicate-dominated (S-type) cosmic spherules among the Monte dei Corvi sediments is consistent with the findings of other studies (e.g. Voldman et al., 2013; Tomkins et al., 2016; Kadyrov et al., 2020) that searched marine sedimentary rocks across the geological sequence. The absence (or low abundance) of silicate-bearing micrometeorites among fossil micrometeorite collections is well-documented and reflects the high susceptibility of silicate minerals to corrosion and dissolution whilst exposed to seawater (silica being undersaturated everywhere in the oceans [Nelson et al., 1995]). This is confirmed by the passive increase in I-type cosmic spherules relative abundances to S-type spherules reported from deep-sea micrometeorite collections (Murray and Renard, 1891; Blanchard and Davis, 1978; Murrell et al., 1980; Savelyev et al., 2022).

5.2. Identification of I-type micrometeorites and alteration during fossilisation

I-type micrometeorites range in diameter from ~50–700 μm (Suavet et al., 2009b) and are formed by the oxidation of chondritic metal (kamacite and taenite) dust during atmospheric entry (Genge et al., 2017). Rapid melting results in the formation of spherical particles while subsequent oxidation progressively converts metal into metal-oxide. This leads to the development of a layered internal structure, with a metal bead encapsulated by an oxide shell. As the metal is oxidized the bead volume decreases while the volume of the oxide shell increases. If entry heating continues, the entire particle will be oxidized to form metal-oxide sphere. This evolution in I-type mineralogy provides the basis for their classification into metal-bearing (MET) and oxidized (OX) subtypes (Genge et al., 2017). Due to the higher oxidation potential of Ni, relative to Fe, the oxide shell is preferentially Fe-enriched. Meanwhile, the metal bead becomes passively enriched in Ni, resulting in some beads composed of >80 wt% Ni. Upon cooling, the particle crystalizes. The metal-oxide melt forms both wüstite and magnetite although the exact ratio and petrographic relationships of these two phases depend on the degree of oxidation experienced. Non-equilibrium effects in the exchange of Ni between wüstite and metal, and magnetite and wüstite result in the presence of characteristic chemical compositions: MET spherules contain Ni-poor (<1.5 wt%) wüstite and Fe-Ni-metal (10–95 wt% Ni) and minor quantities of Ni-free magnetite that occur as a rim along the particle perimeter. Conversely, OX spherules contain Ni-rich wüstite (0.5–22.5 wt%) and magnetite with minimal Ni (often below detection limits) (Genge et al., 2017).

In fully, oxidized spherules PGNs precipitate from the oxide melt and are found as micron-sized accessory phases. They are typically located at the interstices between grains. Furthermore, I-type micrometeorite also typically contain irregular-shaped vesicles representing volume reductions during crystallization, leading to internal void space (Feng et al., 2005). By understanding the formation process of I-types and documenting their petrographic properties we can confidently identify I-type micrometeorites recovered from sedimentary rocks.

The Fe-oxide particles found in the Monte dei Corvi sediments are consistent with I-type micrometeorites, based upon their particle size (<400 μm), the retention of characteristic quenched dendritic textures, the preservation of intact metal beads in some particle (or subspherical cavities representing where former metal beads were dissolved by terrestrial fluids), their high-temperature oxidized mineralogy (including metastable wüstite), the presence of rounded micron-sized PGNs located within the oxide shell (Rudraswami et al., 2011), the presence of Ni-bearing wüstite (0.5–22.5 wt% [Genge et al., 2017]), and chondritic bulk Ni/Co (wt.%/wt.%) ratios (~15–20 [Table 3]) (Folco and Cordier, 2015; Suttle and Genge, 2017). However, the Monte dei Corvi I-types also exhibit clear evidence of alteration owing to interaction with terrestrial fluids.

5.2.1. Geochemical exchange

Chemical analysis of modern Antarctic I-type spherules reveals compositions dominated by Fe, Ni, and O, with detectable quantities of Co and Cr (Table 2 in Genge et al., 2017). Although most of the Monte dei Corvi fossil micrometeorites have Ni, Co and Cr within the ranges observed of unaltered Antarctic spherules, some particles lack detectable Ni, Co or Cr (e.g. particle D5, Table 3). The absence of all three elements is uncharacteristic and suggests loss by leaching. By contrast the Monte dei Corvi spherules may also contain low concentrations of lithophile cations (Na, Mg, Al, Si, Ca, Ti and Mn). With the exception of Mn, these elements occur at low abundances < 0.5 wt% and have a combined total abundance typically < 1.5 wt% (Table 3). Although Mn concentrations are usually low (0.1–0.3 wt%), they are generally elevated relative to the host sediment (~0.1 wt% level [Table S1]) and occur at considerably higher abundances (12–17 wt%) in some particles (A2, A3 and E2). EDX mapping (Fig. 4 of particle A2, Fig. S6 of particle D2) demonstrates that lithophile elements (except Mn) are located primarily within the interstitial areas between Fe-oxide dendrites. These are interpreted as silicate weathering products that were deposited within void spaces.

The implantation of Mn and other cations was previously observed by Suttle and Genge (2017) in fossil I-types recovered from a Cretaceous chalk host rock. The occurrence of essentially the same geochemical signature in micrometeorites preserved at distinctly different time periods (~8.5 Ma vs. 87 Ma) and suggests that this effect is a characteristic feature of fossil micrometeorites deposited in marine settings, or at least those preserved in deep-sea carbonate rocks.

The implantation of lithophile cations into Fe/Ni-oxide minerals depends on the ability of cations to substitute for $Fe^{2+/3+}$ and Ni^{2+} in the crystal structure of wüstite and magnetite. Direct substitution by cations of the same charge and similar ionic radii (e.g. Mn^{2+}, Mg^{2+}, Ca^{2+} and Al^{2+}) can be accommodated relatively easily with small changes in the lattice structure. By contrast, addition of Si^{4+} and Ti^{4+} are more difficult to accommodate and explains their low abundances (Bosi et al., 2009). The behaviour of Mn is distinct from the other cations as its concentrations can reach up to 16.6 wt%. This is similar to the Cretaceous chalk spherules, which also showed high Mn concentrations in some particles (Mn < 9.9 wt%). Manganese is a lithophile element whose 2^+ cation has a similar ionic radius to that of Fe^{2+} (61 pm vs. 67 pm) (Shannon, 1976). Manganese is, therefore, compatible in the wüstite and magnetite structure, with effectively the same substitution capacity as Ni^{2+} (69 pm).

The presence of Mn appears to be a characteristic feature of terrestrially altered fossil micrometeorites. This style of alteration may originate either during interaction with seafloor bottom waters (where ferromanganese crust development occurs, and Mn-rich polymetallic nodules are formed), or by interaction with pore waters during diagenesis. Analysis of the Monte dei Corvi particles alone cannot discern between these two options. However, comparison against geologically modern (unfossilized) I-type cosmic spherules recovered from unconsolidated deep-sea sediments could provide further indication. Manganese was not detected in I-type micrometeorites collected from deep-sea sediments at three sites, including one extracted from ferromanganese crusts in the Pacific Ocean (Bonte et al. 1987; Rudraswami et al., 2014; Savelyev et al., 2022) although other probable deep-sea I-type micrometeorites (Agarwal and Palayil, 2022) do have low but elevated Mn concentrations suggesting that implantation can occur in deep-sea settings but is likely enhanced significantly during diagenesis. Future study on deep-sea micrometeorites is required to accurately determine the timing and origin of Mn additions into I-type micrometeorites.

5.2.2. Replacement of wüstite

In particles B1, D2 and E1 the wüstite phase appears as a mass of submicron crystals with re-entrant interconnected pore-spaces and fractures (Fig. 3C). These textures are indicative of corrosion (Fig.7 in Demoulin et al. (2010)). Meanwhile in particles A3 and D1 wüstite is absent and, instead, they are composed of magnetite plus a different phase, either calcite, ankerite. This additional phase occupies the regions within the particle where wüstite is expected to occur – dispersed through the particle in close association with the magnetite. Furthermore, these additional phases contain minor quantities of Ni. Both features strongly suggest that the calcite/ankerite are secondary replacement minerals that have formed after dissolution of wüstite. Particle E2, is composed exclusively of magnetite. However, it's internal texture preserves the characteristic OX appearance, with two phases discernible: (1) magnetite forming the rim along the particle perimeter and present as cellular dendrites within the particle interior and (2) magnetite in the particle interior acting as the host phase in which the dendrites are suspended. This is interpreted as two distinct generations of magnetite: primary magnetite that formed during atmospheric entry and secondary magnetite that formed by replacement of wüstite after the particles were deposited on the seafloor. The two magnetite

generations have subtly different compositions (Table 3), with the primary magnetite having slightly elevated Ni and Co contents (0.96 and 0.32 wt% respectively) when compared to the secondary magnetite (Ni: 0.60 wt% and Co: 0.19 wt%).

Wüstite is metastable at low temperatures (<570 °C) (Genge et al., 2017) and susceptible to dissolution by fluids, being weakly soluble in acidic waters (Jang and Brantley, 2009). Thus, it is unsurprising that we observe evidence of wüstite dissolution (porous textures in particles B1, D2 [Fig. S6] and E1) and replacement by secondary minerals. The infilling of voids left by wüstite dissolution is analogous to the fossilisation processes that preserve biological specimens in sedimentary rocks and, alongside the occurrence of fossilized ordinary chondrite meteorites in Ordovician limestones (Nyström and Wickman, 1991) further demonstrates that extraterrestrial materials can become fossilized (as opposed to simply being preserved unaltered).

Replacement by calcite is consistent with the host lithology (carbonate muds), while the presence of ankerite (in particle D1) implies that some of the Fe liberated from the dissolution of wüstite remained in the pore space and was then repurposed during carbonate formation to form an Fe-Ca-bearing carbonate. Conversely, in particle E2 wüstite was replaced by a second-generation of magnetite. The high Fe content of magnetite suggests an alternative preservation route. Rather than dissolution and replacement, the magnetite likely instead formed by oxidative recrystallization:

$$3Fe_{(1-x)}O[s] + ½O_2[aq.] \rightleftharpoons Fe_3O_4[s] \quad [\text{Where: } x < 0.2] \tag{1}$$

Note: the added oxygen ($½O_2$[aq.]) would be derived from seawater, while the oxygen in the wüstite ($3Fe_{(1-x)}O$[s]) would be derived from the atmosphere. This mixed heritage has implications for the study of fossil micrometeorites from the geological record and their O-isotope compositions (Section 6).

5.3. Absence of a Veritas signal in the micrometeorite record

Monte dei Corvi beach section represents a site of continuous deposition uninterrupted by sudden changes in palaeoenvironment and unaffected by significant tectonic overprinting. There is minimal change in bulk-rock composition across the studied stratigraphic interval (Table S1 [especially over the range A-D]). Sedimentation rates for the Monte dei Corvi basin were high and fairly stable (11.8 m/Ma [Montanari et al., 2017]). Thus, the sequence investigated in this study is near-ideal for an investigation into the cosmic dust flux, since external factors such as changes in palaeo-environment, sediment input or sedimentation rate were not varying. Likewise the preservation potential of micrometeorites (their chance of becoming fossilized) across this sequence is likely to have been constant, and the techniques used to extract micrometeorites were consistent. This means that potential biases affecting the accumulation and recovery of micrometeorites affect all five sedimentary horizons equally. Therefore, changes in the abundance of fossil micrometeorites between the five sedimentary horizons may reflect changes in the global flux of extraterrestrial material to Earth.

This study was motivated by the discovery of a pronounced increase in extraterrestrial ^{3}He in rocks from the Monte dei Corvi beach section, interpreted as a time period of enhanced cosmic dust flux and associated with the formation of the Veritas asteroid family (Montanari et al., 2017). We set out to test the hypothesis that: "*The period of enhanced ^{3}He input will be detectable in the fossil micrometeorite record.*" To validate this hypothesis our data would need to show a statistically robust difference in either composition, abundance and/or particle size of fossil micrometeorites between the background samples (A and B) and the intra-^{3}He peak samples (C, D and E).

We have already noted that there is no resolvable difference in composition between the two populations (Section 5.1). Furthermore, owing to the small number of micrometeorites recovered at each horizon the variability in micrometeorite abundance across the stratigraphic range cannot be analysed by statistical means. However, analysis of micrometeorite size distribution (particle diameters) between the background (samples A+B) and the intra-^{3}He peak population (samples C+D+E) is possible. We used a Mann-Witney *U* test to explore this relationship. Briefly, this is a nonparametric test used to evaluate the null hypothesis that two independent samples are not statistically resolvable. If the resulting *U*-value is less than a critical value (available in *U*-tables), the null hypothesis can be rejected, and the two samples are deemed statistically resolvable. As in many statistical tests the associated *p*-value provides a measure of the probability that this result is due to chance alone.

For the Monte dei Corvi data (given in Table 2) the calculated *U*-value is 30.5, while the critical value of *U* at $p < 0.05$ is 17. Additionally, the associated *p*-value is 0.36. This result is, therefore, not significant at the $p < 0.05$ interval, meaning that the data collected here do not provide sufficient evidence of a change in the size of cosmic dust reaching Earth (and becoming preserved in the rock record). Therefore, we find no clear relationship between the ^{3}He abundances reported by Montanari et al. (2017) and the fossil micrometeorite populations reported in this study. Our data suggest that fossil (I-type) micrometeorites, at least in the Monte dei Corvi sediments, are not the main carrier phase for extraterrestrial ^{3}He.

5.4. Carrier phases of extraterrestrial ^{3}He in marine sediments

Past measurements of ^{4}He concentrations (and by inference, ^{3}He concentrations) (ng/g) in different types of cosmic dust (Fig. 6) have demonstrated that the smallest size fractions (IDPs) and particles which experienced minimal heating during atmospheric entry (unmelted fine-grained micrometeorites) contain the highest ^{4}He concentrations. However, between 0.01 and 10% of the original ^{3}He is retained in heated cosmic spherules, including within I-type particles (Fig. 6). Once cosmic dust reaches the seafloor and is incorporated into sedimentary rocks the behaviour of ^{3}He remains unknown. It is possible that ^{3}He is leached and redeposited in alternative carrier phases.

Mukhopadhyay and Farley (2006) and later Stuart and Lee (2012) investigated marine sediments with the aim of constraining the carrier phases of extraterrestrial ^{3}He. Stepped heating and leaching experiments demonstrated that most of the ^{3}He in marine sediments was released at temperatures between 600 and 800 °C and that acid-leaching reduced the ^{3}He content of marine sediments by ~70%. As a result, a metallic or Fe-oxide phase (consistent with the mineralogy of the I-type spherules) appeared the most likely carrier of the ^{3}He signature. At Monte dei Corvi, Montanari et al. (2017) also reported a correlation between ^{3}He levels and Ni/Sc, Co/Sc and Cr/Sc (normalization against Sc acts as a tracer of the terrigenous component), implying that metal or metal-oxide component could be the carrier phase of the ^{3}He. However, the data presented in this study (low abundances of I-type micrometeorites, a lack of evidence for a change in the I-type flux, and a lack of fine-grained metal/metal-oxide or IDP material in the smallest size fractions (Fig. S3)) strongly suggests that the original cosmic dust grains liberated from the Veritas break-up event no longer survive. Instead, their geochemical signatures have been re-deposited within, or adhered to a terrestrial mineral phase.

6. Implications – developing fossil I-types as a palaeoclimate proxy

Fossil I-type micrometeorites have the potential to be used as a palaeoclimate proxy, capable of providing quantitative insights into the concentration of oxygen (pO_2) in Earth's upper atmosphere over geological time (Tomkins et al., 2016; Pack et al., 2017; Lehmer et al., 2020; Fischer et al., 2021; Huang et al., 2021). This is because I-type cosmic spherules represent fragments of chondritic metal (kamacite and taenite) that are oxidized and melted during atmospheric entry (Genge

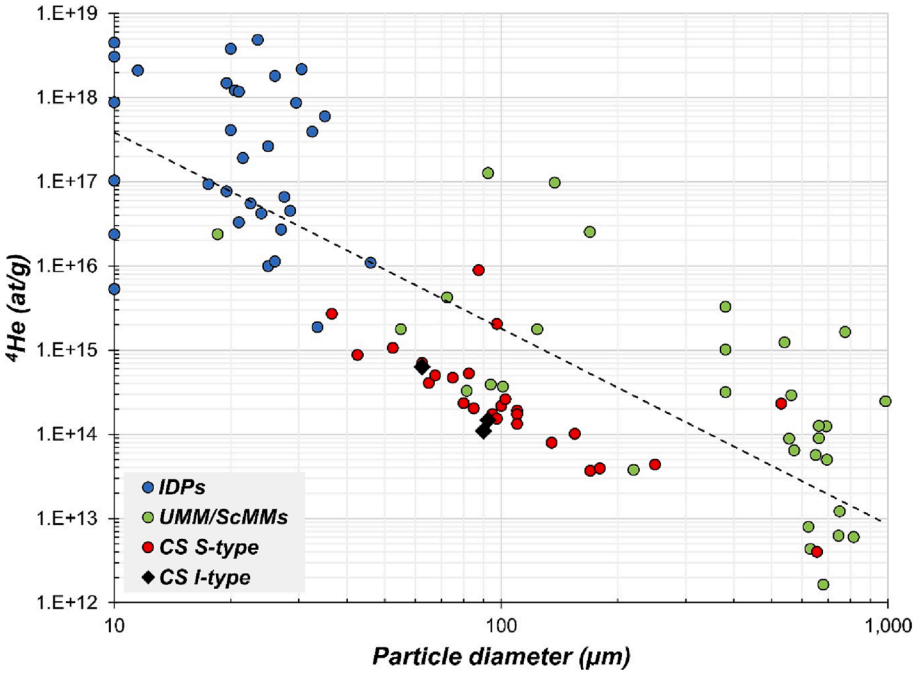

Fig. 6. Concentration of helium measured in different types of cosmic dust. Here ^{4}He (at/g) is just as a proxy for the lower abundance ^{3}He isotope. Cosmic dust subtypes are distinguished by symbol colour and shape: IDPs are shown in blue, unmelted and scoriaceous micrometeorites are shown in green, S-type cosmic spherules are shown in red, and I-type cosmic spherules are denoted by black diamonds. A dashed black trendline demonstrates the power law relationship between particle size (diameter) and ^{4}He concentration. The smallest particles (IDPs) contain the highest ^{4}He concentrations. In addition, the degree of thermal processing during atmospheric entry also controls ^{4}He concentrations. Melting during entry results in a significant loss of volatile helium, as demonstrated by the lower concentrations measured in cosmic spherules. Only three data points exist for I-type micrometeorites (all modern, Antarctic samples). Data were obtained from the literature (Osawa et al., 2003; Kehm et al., 2006; Baecker et al., 2018; Baecker et al., 2022).

et al., 2017). As a result, all of the oxygen present in I-type spherules derives from Earth's atmosphere. This means that the O-isotope composition of Earth's past atmosphere could be inferred by measuring fossil I-type spherules (Pack et al., 2017; Fischer et al., 2021) and correcting for the effects of mass-dependent fractionation arising during high-temperature heating (Suavet et al., 2010; Lampe et al., 2022). Additionally, the degree of oxidation among a large population of fossil I-type spherules could be used to probe the composition of Earth's atmosphere in the past. The oxidation state is directly related to pO_2 in the upper atmosphere, allowing micrometeorites to provide a measure of the oxidative capacity of Earth's atmosphere in the geological past.

However, before fossil I-types can be effectively used as a climate proxy we must understand the alteration history and the preservation of individual spherules, both on the seafloor and during diagenesis, as the host sediments are converted to a sedimentary rock. Our investigation of the Monte dei Corvi fossil micrometeorites, alongside previous studies on fossil micrometeorites from Cretaceous chalk (Suttle and Genge, 2017) and Archean sandstones (Tomkins et al., 2016) provides key insights into how cosmic dust is altered and how this may impact any interpretations drawn from their analysis.

The presence of second-generation magnetite, formed by the recrystallization of wüstite in one of the Monte dei Corvi spherules (particle E2 [Fig. 3G and H]) represents a potential problem for the use of fossil micrometeorites as a palaeoclimate proxy because observations of mineralogy, textures and potentially O-isotope composition could be due to either atmospheric entry or post-depositional alteration. Thus, it is critical to assess how common recrystallization may be among fossil micrometeorite collections and whether altered fossil I-types can be confidently discerned or otherwise accounted for.

Almost every fossil I-type spherule reported by Suttle and Genge (2017) from a Cretaceous chalk host rock were found to be single-phase low-Mn magnetite with relatively featureless interiors dominated by cellular dendrites. Similar particle textures (without reports of chemical composition) were observed from modern I-type spherules recovered from the Pacific Ocean (Stuart and Lee, 2012). Given the above observation (in particle E2) that wüstite can be altered to magnetite during terrestrial residence, we can conclude that many of the Cretaceous chalk micrometeorites (and Pacific Ocean particles) were originally mixed phase OX spherules composed of wüstite and magnetite and whose wüstite portion was subsequently recrystallized. This implies that the wüstite-to-magnetite conversion is a common process, at least in some rock types. There are two implications of this discovery:

1. If the wüstite-to-magnetite recrystallization reactions leave little textural clues, preventing the distinction between atmospheric and depositional magnetite populations (as appears the case from the Cretaceous chalk spherules, and to a lesser extent from particle E2 in the Monte dei Corvi collection), then the pre-depositional mineralogy of fossil I-type spherules will be more difficult to reconstruct. Assuming that the different Fe-oxide phases cannot be confidently discerned in fossil I-type spherules, researchers analysing future collections will still be able to classify their I-type micrometeorites into MET and OX subgroups. This is because evidence of metal beads is retained either as direct retention of metal (as in particle A2 [Fig. 3A]) or retention of a large subspherical cavity (as in particle C3 [Fig. 3B]) representing the site of a former metal bead. This is a critical capability because the ratio of MET to OX spherules provides an assessment of the relative oxidative capacity of Earth's atmosphere at the time of their arrival on Earth. Thus, by comparing the MET-to-OX ratio of large numbers of I-types (e.g. N > 100) from fossil collections against a statistically representative population of modern I-types we will be able to obtain a quantitative assessment of the relative change in oxidation potential of Earth's atmosphere at discrete time periods in Earth's history. This knowledge provides the tools necessary to continue developing fossil micrometeorites as a climate proxy.
2. Wüstite-to-magnetite replacement reactions occurring on the seafloor will affect the oxygen content of recrystallized fossil micrometeorites. We predict that these altered cosmic spherules will be a mix of oxygen derived from the upper atmosphere and oxygen derived from seawater/diagenetic porewater (shown in e.q.1). Textural analysis is, therefore, crucial for distinguishing primary from secondary oxygen carriers. Furthermore, spatially-resolved SIMS measurements (δ^{18}O) on sectioned fossil I-types could be used to test whether deep-sea and fossil micrometeorites preserve end-member O-isotope compositions (atmosphere and ocean bottom signatures) or any evidence of mixing due to solid-state diffusion processes. The potential mixed heritage of oxygen in fossil

micrometeorites means that fossil I-type micrometeorites cannot be interpreted as a reflection of their atmospheric entry history unless solid-state recrystallization reactions can be confidently excluded.

7. Conclusions

7.1. Testing the Veritas hypothesis

This study recovered 20 fossil I-type micrometeorites from 118.9 kg of carbonate muds (marls) with ages between ~8.7–7.9 Ma ago. The time span includes sediments deposited before, and during the ^{3}He peak previously identified by Farley et al. (2006) and Montanari et al. (2017). Our aim was to extract fossil micrometeorites from across the stratigraphic section and to determine if they were related to the Veritas asteroid family. The lack of a clear change in micrometeorite concentration, size or composition across the five sedimentary horizons studied suggests that the recovered micrometeorites are samples of the background flux of extraterrestrial material. Furthermore, because there is no clear evidence for a Veritas signal, this suggests that the Veritas family is composed of highly friable materials and that Fe-Ni-metal grains and Cr-spinel grains (Boschi et al., 2019) are relatively minor components (or indeed absent) from this group. Based on these constraints, the current hypothesis that the Veritas family is composed of hydrated carbonaceous chondrite material is supported. Indeed, the low abundance I-type spherules in combination with a ^{3}He peak provides positive evidence by which influxes of extraterrestrial material with low contents of ferrous metal grains can be identified.

7.2. The fossilisation of cosmic dust and the use of micrometeorites as an atmospheric proxy

The recovery of fossil micrometeorites from the Monte dei Corvi sediments further demonstrates that fragments of chondritic metal are relatively common in the geological record, that they can be preserved in the marine rock record and subsequently identified even where alteration has affected their mineralogy, textures, and chemical composition.

Post-depositional alteration is characterised by leaching of Ni, Co and Cr and implantation of lithophile cations (typically Mn at abundances < 17 wt% and potentially also low concentrations of Na, Al, Si, Mg and Ca). Because Mn mineralisation is a common process on the seafloor, we suggest that the solid-state geochemical exchange processes most likely occur on the seafloor although diagenetic processes may have played a role.

The other alteration feature, observed in some micrometeorites, was the dissolution of wüstite and replacement by a terrestrial phase (calcite or ankerite), or the recrystallization of wüstite into a second generation of magnetite. This later process could limit the viability of fossil micrometeorites as a palaeo-climate proxy if care is not taken to accurately characterise the preservation characteristics of fossil micrometeorites recovered from sedimentary rocks. However, where secondary processes have altered the Fe-oxide mineralogy and textures, it remains possible to discriminate metal-bearing (MET) I-type spherules from fully oxidized (OX) spherules. As a result, the ratio of MET-to-OX particles among a large, statistically significant population of fossil micrometeorites could be used to quantitatively evaluate the oxidative capacity of Earth's atmosphere in the geological past (pO_2). In conclusion, fossil micrometeorites remain a viable upper atmosphere palaeo-climate proxy, providing sufficient developmental research is conducted.

Declaration of Competing Interest

The authors declare that they have no known competing financial interests or personal relationships that could have appeared to influence the work reported in this paper.

Acknowledgements

Fieldwork was facilitated by a generous research grant from the Royal Society Research (grant number: RGS-R1-221005). Funding for micrometeorite research at the University of Pisa is facilitated by the Italian Programma Nazionale delle Ricerche in Antartide (PNRA) under grant number PNRA16 00029.

Appendix A. Supplementary material

These include images of the non-magnetic separates, SEM images of the <63 μm size fractions (search for IDP material), images of the equipment used in the processing of sediments for micrometeorite extraction and SEM images of all micrometeorites (exteriors and interiors) Supplementary material to this article can be found online at https://doi.org/10.1016/j.gca.2023.06.027.

References

Agarwal, D.K., Palayil, J.K., 2022. Recovery of hydrothermal wustite-magnetite spherules from the Central Indian Ridge, Indian Ocean. Sci. Rep. 12, 6811.
Baecker, B., Ott, U., Cordier, C., Folco, L., Trieloff, M., Van Ginneken, M., Rochette, P., 2018. Noble gases in micrometeorites from the Transantarctic Mountains. Geochim. Cosmochim. Acta 242, 266–297.
Baecker, B., Ott, U., Trieloff, M., Engrand, C., Duprat, J., 2022. Noble gases in Dome C micrometeorites-An attempt to disentangle asteroidal and cometary sources. Icarus 376, 114884.
Blanchard, M.B., Davis, A.S., 1978. Analysis of ablation debris from natural and artificial iron meteorites. J. Geophys. Res. Solid Earth 83, 1793–1808.
Bonté, P., Jehanno, C., Maurette, M., Brownlee, D.E., 1987. Platinum metals and microstructure in magnetic deep sea cosmic spherules. J. Geophys. Res. 92, E641–E648.
Boschi, S., Schmitz, B., Montanari, A., 2019. Distribution of chrome-spinel grains across the ^{3}He anomaly of the Tortonian Stage at the Monte dei Corvi section, Italy. *Geol. Soc. Am. Spec.* 542, 383–391.
Bosi, F., Hålenius, U., Skogby, H., 2009. Crystal chemistry of the magnetite-ulvospinel series. Am. Min. 94, 181–189.
Bottke, W.F., Brož, M., O'Brien, D.P., Bagatin, A.C., Morbidelli, A., Marchi, S., 2015. The collisional evolution of the main asteroid belt. In: Michel, P., DeMeo, F.E., Bottke, W. F. (Eds.), Asteroids IV. Univ. of Arizona, Tucson, pp. 701–724.
Cleaveland, L.C., Jensen, J., Goese, S., Bice, D.M., Montanari, A., 2002. Cyclostratigraphic analysis of pelagic carbonates at Monte dei Corvi (Ancona, Italy) and astronomical correlation of the Serravallian-Tortonian boundary. Geology 30, 931–934.
Darken, L., Gurry, R.W., 1946. The system iron—oxygen. II. Equilibrium and thermodynamics of liquid oxide and other phases. J. Am. Chem. Soc. 68, 798–816.
Delbo, M., Avdellidou, C., Morbidelli, A., 2019. Ancient and primordial collisional families as the main sources of X-type asteroids of the inner main belt. Astron. Astrophys. 624, A69.
DeMeo, F.E., Carry, B., 2014. Solar System evolution from compositional mapping of the asteroid belt. Nature 505, 629–634.
DeMeo, F.E., Binzel, R.P., Slivan, S.M., Bus, S.J., 2009. An extension of the Bus asteroid taxonomy into the near-infrared. Icarus 202, 160–180.
Demoulin, A., Trigance, C., Neff, D., Foy, E., Dillmann, P., L'Hostis, V., 2010. The evolution of the corrosion of iron in hydraulic binders analysed from 46-and 260-year-old buildings. Corros. Sci. 52, 3168–3179.
Farley, K.A., 1995. Cenozoic variations in the flux of interplanetary dust recorded by ^{3}He in a deep-sea sediment. Nature 376, 153–156.
Farley, K.A., Vokrouhlický, D., Bottke, W.F., Nesvorný, D., 2006. A late Miocene dust shower from the break-up of an asteroid in the main belt. Nature 439, 295–297.
Feng, H., Jones, K.W., Tomov, S., Stewart, B., Herzog, G.F., Schnabel, C., Brownlee, D.E., 2005. Internal structure of type I deep-sea spherules by X-ray computed microtomography. Meteorit. Planet. Sci. 40, 195–206.
Fischer, M.B., Oeser, M., Weyer, S., Folco, L., Peters, S.T., Zahnow, F., Pack, A., 2021. I-Type Cosmic Spherules as Proxy for the Δ'^{17}O of the Atmosphere—A Calibration With Quaternary Air. Paleoceanogr Paleoclimatol. 36 e2020PA004159.
Folco, L., Cordier, C., 2015. Micrometeorites. EMU Notes in Mineralogy. In: Lee, M.R., Leroux, H. (Eds.). Planetary Mineralogy. European Mineralogical Union, The Mineralogical Society of Great Britain and Ireland, vol. 15, pp.253–297 (Chap. 9).
Fornasier, S., Lantz, C., Barucci, M.A., Lazzarin, M., 2014. Aqueous alteration on main belt primitive asteroids: Results from visible spectroscopy. Icarus 233, 163–178.
Genge, M.J., Davies, B., Suttle, M.D., van Ginneken, M., Tomkins, A.G., 2017. The mineralogy and petrology of I-type cosmic spherules: Implications for their sources, origins and identification in sedimentary rocks. Geochim. Cosmochim. Acta 218, 167–200.
Greenwood, R.C., Schmitz, B., Bridges, J.C., Hutchison, R., Franchi, I.A., 2007. Disruption of the L chondrite parent body: new oxygen isotope evidence from Ordovician relict chromite grains. Earth Planet. Sci. Lett. 262, 204–213.
Greenwood, R.C., Burbine, T.H., Franchi, I.A., 2020. Linking asteroids and meteorites to the primordial planetesimal population. Geochim. Cosmochim. Acta 277, 377–406.

Heck, P.R., Ushikubo, T., Schmitz, B., Kita, N.T., Spicuzza, M.J., Valley, J.W., 2010. A single asteroidal source for extraterrestrial Ordovician chromite grains from Sweden and China: High-precision oxygen three-isotope SIMS analysis. Geochim. Cosmochim. Acta 74, 497–509.
Herbert, T.D., Lawrence, K.T., Tzanova, A., Peterson, L.C., Caballero-Gill, R., Kelly, C.S., 2016. Late Miocene global cooling and the rise of modern ecosystems. Nat. Geosci. 9, 843–847.
Hilgen, F.J., Aziz, H.A., Krijgsman, W., Raffi, I., Turco, E., 2003. Integrated stratigraphy and astronomical tuning of the Serravallian and lower Tortonian at Monte dei Corvi (Middle–Upper Miocene, northern Italy). Palaeogeogr. Palaeoclimatol. Palaeoecol. 199, 229–264.
Hilgen, F., Aziz, H.A., Bice, D., Iaccarino, S., Krijgsman, W., Kuiper, K., Montanari, A., Raffi, I., Turco, E., Zachariasse, W.J., 2005. The global boundary stratotype section and point (GSSP) of the Tortonian stage (Upper Miocene) at Monte Dei Corvi. Epi. J. Int. Geosci. 28, 6–17.
Hirayama, K., 1918. Groups of asteroids probably of common origin. Proc. Tokyo Mathematico-Phys. Soc. 9, 354–361.
Huang, G., Eager, J.K., Mayne, N.J., Cui, D., Manners, J., Hebrard, E., Liu, Z., Lenton, T. M., 2021. CO_2 and O_2 oxidized 2.7 Ga micrometeorites in two stages suggesting a> 32% CO_2 atmosphere. Precambrian Res. 366, 106423.
Hüsing, S.K., Kuiper, K.F., Link, W., Hilgen, F.J., Krijgsman, W., 2009a. The upper Tortonian–lower Messinian at Monte dei Corvi (Northern Apennines, Italy): completing a Mediterranean reference section for the Tortonian stage. Earth Planet. Sci. Lett. 282, 140–157.
Hüsing, S.K., Dekkers, M.J., Franke, C., Krijgsman, W., 2009b. The Tortonian reference section at Monte dei Corvi (Italy): evidence for early remanence acquisition in Miocene-bearing sediments. Geophys. J. Int. 179, 125–143.
Jang, J.H., Brantley, S.L., 2009. Investigation of Miocene (FeO) dissolution: Implications for reductive dissolution of ferric oxides. Environ. Sci. Technol. 43, 1086–1090.
Kadyrov, R., Glukhov, M., Statsenko, E., Galliulin, B., 2020. Enigma of ferruginous inclusions in Permian evaporites. Arab. J. Geosci. 13, 1–17.
Kaluna, H.M., Masiero, J.R., Meech, K.J., 2016. Space weathering trends among carbonaceous asteroids. Icarus 264, 62–71.
Kehm, K., Flynn, G.J., Hohenberg, C.M., 2006. Noble gas space exposure ages of individual interplanetary dust particles. Meteorit. Planet. Sci. 41, 1199–1217.
Korochantseva, E.V., Trieloff, M., Lorenz, C.A., Buykin, A.I., Ivanova, M.A., Schwarz, W. H., Hopp, J., Jessberger, E.K., 2007. L-chondrite asteroid breakup tied to Ordovician meteorite shower by multiple isochron ^{40}Ar-^{39}Ar dating. Meteorit. Planet. Sci. 42, 113–130.
Lampe, S., Soens, B., Chernonozhkin, S.M., de Vega, C.G., van Ginneken, M., Van Maldeghem, F., Vanhaecke, F., Glass, B.P., Franchi, I.A., Terryn, H., Debaille, V., 2022. Decoupling of chemical and isotope fractionation processes during atmospheric heating of micrometeorites. Geochim. Cosmochim. Acta 324, 221–239.
Lehmer, O.R., Catling, D.C., Buick, R., Brownlee, D.E., Newport, S., 2020. Atmospheric CO_2 levels from 2.7 billion years ago inferred from micrometeorite oxidation. Sci. Adv. 6, eaay4644.
Lindskog, A., Costa, M.M., Rasmussen, C.Ø., Connelly, J.N., Eriksson, M.E., 2017. Refined Ordovician timescale reveals no link between asteroid breakup and biodiversification. Nat. Commun. 8, 1–8.
Mackinnon, I.D., Rietmeijer, F.J., 1987. Mineralogy of chondritic interplanetary dust particles. Rev. Geophys. 25, 1527–1553.
Meier, M.M.M., Schmitz, B., Baur, H., Wieler, R., 2010. Noble gases in individual L chondritic micrometeorites preserved in an Ordovician limestone. Earth Planet. Sci. Lett. 290, 54–63.
Merrihue, C., 1965. Rare gas evidence for cosmic dust in modern Pacific red clay. Ann. N. Y. Acad. Sci. 119, 351–367.
Michel, P., Jutzi, M., Richardson, D.C., Benz, W., 2011. The Asteroid Veritas: An intruder in a family named after it? Icarus 211, 535–545.
Montanari, A., Beaudoin, B., Chan, L.S., Coccioni, R., Deino, A., DePaolo, D.J., Emmanuel, L., Fornaciari, E., Kruge, M., Lundblad, S., Mozzato, C., 1997. Chapter E1 Integrated stratigraphy of the middle to upper miocene pelagic sequence of the Conero Riviera (Marche region, Italy). In: Developments in Palaeontology and StratigraphyElsevier., vol. 15, pp. 409–450.
Montanari, A., Farley, K., Claeys, P., De Vleeschouwer, D., De Winter, N., Vansteenberge, S., Sinnesael, M., Koeberl, C., 2017. Stratigraphic record of the asteroidal Veritas breakup in the Tortonian Monte dei Corvi section (Ancona, Italy). Geol. Soc. Am. Bull. 129, 1357–1376.
Morbidelli, A., Walsh, K.J., O'Brien, D.P., Minton, D.A., Bottke, W.F., 2015. The dynamical evolution of the asteroid belt. In: Michel, P., DeMeo, F.E., Bottke, W.F. (Eds.), Asteroids IV. Univ. of Arizona, Tucson, pp. 493–507.
Mukhopadhyay, S., Farley, K.A., 2006. New insights into the carrier phase(s) of extraterrestrial ^{3}He in geologically old sediments. Geochim. Cosmochim. Acta 70, 5061–5073.
Murray, J., Renard, A.F., 1891. Report on Deep-sea Deposits Based on the Specimens Collected During the Voyage of HMS Challenger in the Years 1872 to 1876. HM Stationery Office, p. 404.
Murrell, M.T., Davis Jr, P.A., Nishiizumi, K., Millard Jr, H.T., 1980. Deep-sea spherules from Pacific clay: Mass distribution and influx rate. Geochim. Cosmochim. Acta 44, 2067–2074.
Mutch, T.A., 1965. Extraterrestrial particles in Paleozoic salts. Ann. N. Y. Acad. Sci. 119, 166–185.
Nelson, D.M., Tréguer, P., Brzezinski, M.A., Leynaert, A., Quéguiner, B., 1995. Production and dissolution of biogenic silica in the ocean: revised global estimates, comparison with regional data and relationship to biogenic sedimentation. Glob. Biogeochem. Cycles 9, 359–372.
Nesvorný, D., Morbidelli, A., Vokrouhlický, D., Bottke, W.F., Brož, M., 2002. The Flora family: A case of the dynamically dispersed collisional swarm? Icarus 157, 155–172.
Nesvorný, D., Bottke, W.F., Levison, H.F., Dones, L., 2003. Recent origin of the Solar System dust bands. Astrophys. J. 591, 486–497.
Nesvorný, D., Vokrouhlický, D., Bottke, W.F., Sykes, M., 2006. Physical properties of asteroid dust bands and their sources. Icarus 181, 107–144.
Nesvorný, D., Vokrouhlický, D., Morbidelli, A., Bottke, W.F., 2009. Asteroidal source of L chondrite meteorites. Icarus 200, 698–701.
Nyström, J.O., Wickman, F.E., 1991. The Ordovician chondrite from Brunflo, central Sweden, II. Secondary minerals. *Lithos* 27, 167–185.
Onoue, T., Nakamura, T., Haranosono, T., Yasuda, C., 2011. Composition and accretion rate of fossil micrometeorites recovered in Middle Triassic deep-sea deposits. Geology 39, 567–570.
Osawa, T., Nakamura, T., Nagao, K., 2003. Noble gas isotopes and mineral assemblages of Antarctic micrometeorites collected at the meteorite ice field around the Yamato Mountains. Meteorit. Planet. Sci. 38, 1627–1640.
Pack, A., Höweling, A., Hezel, D.C., Stefanak, M.T., Beck, A.K., Peters, S., Sengupta, S., Herwartz, D., Folco, L., 2017. Tracing the oxygen isotope composition of the upper Earth's atmosphere using cosmic spherules. Nat. Commun. 8, 1–7.
Reiners, P.W., Turchyn, A.V., 2018. Extraterrestrial dust, the marine lithologic record, and global biogeochemical cycles. Geology 46, 863–866.
Rudraswami, N.G., Parashar, K., Shyam Prasad, M., 2011. Micrometer-and nanometer-sized platinum group nuggets in micrometeorites from deep-sea sediments of the Indian Ocean. Meteorit. Planet. Sci. 46, 470–491.
Rudraswami, N.G., Prasad, M.S., Babu, E.V.S.S.K., Kumar, T.V., 2014. Chemistry and petrology of Fe–Ni beads from different types of cosmic spherules: Implication for precursors. Geochim. Cosmochim. Acta 145, 139–158.
Rudraswami, N.G., Pandey, M., Genge, M.J., Fernandes, D., 2021. Extraterrestrial dust as a source of bioavailable iron contributing to the ocean for driving primary productivity. Meteorit. Planet. Sci. 56, 2175–2190.
Savelyev, D.P., Savelyeva, O.L., Moskaleva, S.V., Rashidov, V.A., 2022. Composition of Cosmic Spherules from Ferromanganese Crusts of the Magellan Seamounts. Geochem. Int. 60, 411–420.
Schmitz, B., Häggström, T., 2006. Extraterrestrial chromite in Middle Ordovician marine limestone at Kinnekulle, southern Sweden—Traces of a major asteroid breakup event. Meteorit. Planet. Sci. 41, 455–466.
Schmitz, B., Lindström, M., Asaro, F., Tassinari, M., 1996. Geochemistry of meteorite-rich marine limestone strata and fossil meteorites from the lower Ordovician at Kinnekulle, Sweden. Earth Planet. Sci. Lett. 145, 31–48.
Schmitz, B., Peucker-Ehrenbrink, B., Lindström, M., Tassinari, M., 1997. Accretion rates of meteorites and cosmic dust in the Early Ordovician. Science 278, 88–90.
Schmitz, B., Huss, G.R., Meier, M.M., Peucker-Ehrenbrink, B., Church, R.P., Cronholm, A., Davies, M.B., Heck, P.R., Johansen, A., Keil, K., Kristiansson, P., 2014. A fossil winonaite-like meteorite in Ordovician limestone: A piece of the impactor that broke up the L-chondrite parent body? Earth Planet Sci. Lett. 400, 145–152.
Schmitz, B., Farley, K.A., Goderis, S., Heck, P.R., Bergström, S.M., Boschi, S., Claeys, P., Debaille, V., Dronov, A., Van Ginneken, M., Harper, D.A., 2019. An extraterrestrial trigger for the mid-Ordovician ice age: Dust from the breakup of the L-chondrite parent body. Sci. Adv. 5, p.eaax4184.
Schmitz, B., Feist, R., Meier, M.M., Martin, E., Heck, P.R., Lenaz, D., Topa, D., Busemann, H., Maden, C., Plant, A.A., Terfelt, F., 2019. The micrometeorite flux to Earth during the Frasnian-Famennian transition reconstructed in the Coumiac GSSP section, France. Earth Planet. Sci. Lett. 522, 234–243.
Shannon, R.D., 1976. Revised effective ionic radii and systematic studies of interatomic distances in halides and chalcogenides. Acta Crystallogr. 32, 751–767.
Spoto, F., Milani, A., Knežević, Z., 2015. Asteroid family ages. Icarus 257, 275–289.
Stuart, F.M., Lee, M.R., 2012. Micrometeorites and extraterrestrial He in a ferromanganese crust from the Pacific Ocean. Chem. Geol. 322, 209–214.
Suavet, C., Gattacceca, J., Rochette, P., Perchiazzi, N., Folco, L., Duprat, J., Harvey, R.P., 2009a. Magnetic properties of micrometeorites. J. Geophys. Res 114, B04102.
Suavet, C., Rochette, P., Kars, M., Gattacceca, J., Folco, L., Harvey, R.P., 2009b. Statistical properties of the Transantarctic Mountains (TAM) micrometeorite collection. Polar Sci. 3, 100–109.
Suavet, C., Alexandre, A., Franchi, I.A., Gattacceca, J., Sonzogni, C., Greenwood, R.C., Folco, L., Rochette, P., 2010. Identification of the parent bodies of micrometeorites with high-precision oxygen isotope ratios. Earth Planet. Sci. Lett. 293, 313–320.
Suttle, M.D., Genge, M.J., 2017. Diagenetically altered fossil micrometeorites suggest cosmic dust is common in the geological record. Earth Planet. Sci. Lett. 476, 132–142.
Taylor, S., Brownlee, D.E., 1991. Cosmic spherules in the geologic record. Meteorit. 26, 203–211.
Taylor, S., Lever, J.H., Harvey, R.P., 2000. Numbers, types, and compositions of an unbiased collection of cosmic spherules. Meteorit. Planet. Sci. 35, 651–666.
Tomkins, A.G., Bowlt, L., Genge, M., Wilson, S.A., Brand, H.E., Wykes, J.L., 2016. Ancient micrometeorites suggestive of an oxygen-rich Archaean upper atmosphere. Nature 533, 235–238.
Tsiganis, K., Knežević, Z., Varvoglis, H., 2007. Reconstructing the orbital history of the Veritas family. Icarus 186, 484–497.
Van Ginneken, M., Genge, M.J., Folco, L., Harvey, R.P., 2016. The weathering of micrometeorites from the Transantarctic Mountains. Geochim. Cosmochim. Acta 179, 1–31.
Vokrouhlický, D., Nesvorný, D., Bottke, W.F., 2008. Evolution of dust trails into bands. Astrophys. J. 672, 696.

Voldman, G.G., Genge, M.J., Albanesi, G.L., Barnes, C.R., Ortega, G., 2013. Cosmic spherules from the Ordovician of Argentina. Geol. J. 48, 222–235.
Wotzlaw, J.F., Hüsing, S.K., Hilgen, F.J., Schaltegger, U., 2014. High-precision zircon U-Pb geochronology of astronomically dated volcanic ash beds from the Mediterranean Miocene. Earth Planet. Sci. Lett. 407, 19–34.
Ziffer, J., Campins, H., Licandro, J., Walker, M.E., Fernandez, Y., Clark, B.E., Mothe-Diniz, T., Howell, E., Deshpande, R., 2011. Near-infrared spectroscopy of primitive asteroid families. Icarus 213, 538–546.